Determination of pure mode-I fracture toughness of multidirectional composite DCB specimens

Ruodi Jia, Libin Zhao, Rémi Curti, Xiaojing Gong

Determination of pure mode-I fracture toughness of multidirectional composite DCB specimens

Ruodi Jia[1, 2], Libin Zhao[2, *], Curti Rémi[1], Xiaojing Gong[1, *]

1 Université de Toulouse, ICA (Institut Clément Ader), CNRS UMR 5312, UPS, IUT Tarbes, 65000 Tarbes, France

2 School of Astronautics, Beihang University, Beijing 100191, PR China

Abstract

Strain energy release rate (SERR) along a linear crack front of a multidirectional composite DCB specimen shows an obviously non-uniform distribution, which causes the fracture toughness G_{Iavg} measured by experiments smaller than the real G_{IC}, and so leading to a lower estimation of fracture toughness. In this study, based on the numerical model a novel semi-empirical closed-form formula was proposed for determination of pure mode I fracture toughness of a multidirectional composite DCB specimen via a width-wise non-uniform distribution parameter. These expressions translate the relationships between the width-wise non-uniform distribution ratio and the specimen width as well as the material parameters. They provide a rapid method to measure correctly the pure mode I fracture toughness of an uncoupled multidirectional composite DCB specimen by integrating the effect of non-uniform distribution of the strain energy release rate at the crack front.

Keywords: Multidirectional DCB specimen, composite, mode I fracture toughness, width-wise distribution of SERR

Nomenclature

Symbols	Description
a_0	initial crack length (mm)
b	specimen width (mm)
h	Thickness of one arm of DCB specimen (mm)
L	specimen length(mm)
v_{ij}	Poisson's ratio of unidirectional laminate
A_{ij} , $B_{ij,}$ D_{ij}	in-plane, coupling and bending stiffness matrix, respectively
D_c	coupling parameter, $D_c = D_{12}^2/D_{11}D_{22}$
D_{c0}	coupling parameter for unidirectional laminate
E_e	materials elastic properties
E_{ii}	elastic modulus of unidirectional laminate (GPa)
G_{ij}	shear modulus of unidirectional laminate (GPa)
G_I	mode-I strain energy release rate (SERR) (J/mm)
G_{Imax}	maximum value of SERR along the crack front (J/mm)
G_{Iavg}	width-wise average value of SERR along the crack front (J/mm)
G_{IC}, G_{IIC}, G_{IIIC}	fracture toughness under pure mode I, II, III(J/mm)
α	fiber orientation angle (°)
β	non-uniformity ratio for mode-I strain energy release rate, $\beta = G_{Imax}/G_{Iavg}$
β_0	non-uniformity ratio for unidirectional specimen
β_{15}	non-uniformity ratio for specimen with width b = 15mm
β_∞	non-uniformity ratio for specimen with an infinite width
η	anisotropy ratio
k, m, n	fitting parameters of the proposed models
k^*	non-dimensional parameter, $\ln((\beta_{15}- \beta_\infty)/15)$

1. Introduction

Fiber Reinforced Polymer (FRP) laminates are widely used in the primary structure of aircrafts, transportation, and other engineering fields due to their high specific stiffness and

specific strength as well as their design flexibility [1-3]. However, the separation of plies called delamination, as one of the most common failure modes in laminated structures under loadings due to relatively weakness of the interlaminar strength of laminates, causes challenges in these applications. Based on fracture mechanics, the basic modes of delamination include pure mode I (opening), pure mode II (in-plane shear) and pure mode III (out-of-plane shear). According to Griffith's theory the initiation of crack propagation under these pure modes can be characterized by fracture toughness in term of Critical Strain Energy Release Rate (CSERR): G_{IC}, G_{IIC} and G_{IIIC}, respectively. In a laminated composite structure in service, the delamination occurs in general in mixed mode with possible participation of mode I, mode II and mode III altogether. General criterion of mixed mode delamination could be established as a function of a mixed mode ratio and pure mode toughness G_{IC}, G_{IIC} and G_{IIIC} [4-5]. Among them, the delamination under pure mode I loading is more common as a result of the lower fracture energy required for the crack initiation. Thus, abundant experimental and numerical investigations have been conducted on mode I delamination problems.

With lots of efforts, standard experimental method ASTM D5528-13 [6] has been established for Double Cantilever Beam (DCB) tests of unidirectional (UD) composites laminates. This standard test method only focuses on the measurement of pure mode I fracture toughness G_{IC} using UD DCB specimens where G_{IC} is considered as the width-wise average value of G_I at the critical load. However, the multidirectional (MD) laminated composites are more widely applied in practice. The fracture toughness of MD laminate measured by DCB test could be very different from that of UD laminate [7-9]. On one hand, the failure mechanism in the multidirectional laminates is more complicated, some common physical phenomenon like multi-cracking and crack jumping in MD DCB specimens may increase or decrease the fracture toughness measured [10]. On the other hand, the width-wise distribution of mode I SERR of MD DCB specimens is not uniform at all. For laminates made from the same prepreg, this non-uniformity depends not only on the constituent materials, stacking sequence, but also on the geometry of the specimen. In fact, in any uncoupled DCB specimen, the maximum SERR is located at the middle of the width; herein under nearly plane strain

condition the material behavior is more brittle and the crack front needs less energy to grow. Therefore, the crack growth was usually initiated at the middle of the specimen width even for UD DCB specimens.

In previous works [7-8], it is demonstrated that the critical energy release rate G_{IC} should be measured using the maximum SERR instead of the average SERR G_{Iavg} because of the non-uniformity of the SERR. Thus, a characterization parameter, $\beta = G_{Imax}/G_{Iavg}$, in which G_{Imax} and G_{Iavg} denote the maximum and the width-wise average SERR over the specimen's width, respectively, was used for the analysis of SERR non-uniformity distribution. For a UD laminate, the relative difference between G_{Imax} and G_{Iavg} is usually less than 10% (β<110%), it is so logical to take the average value as measured fracture toughness so as to reserve 10% safety margin in engineering application. However, in the cases of MD DCB specimens, the ratio β can be very high, G_{Imax} can be 80% higher than G_{Iavg} (β>180%) for example, then, a width-wise average value G_{Iavg} should be incapable to represent the fracture toughness because the crack initiation occurs always at the points where maximum SERR attains its critical value.

In the literature, the parameters which affect the non-uniformity ratio β have been also investigated. Davidson et al. [11] showed that the non-uniformity is proportional to the parameter D_c, $D_c = D_{12}^2/D_{11}D_{22}$. He pointed that delamination front curvature increases with increasing D_c ratio for a given aspect ratio [12] and the value of D_c can be minimized through choosing proper stacking sequence of MD DCB specimen [10-14]. It was proposed that when D_c < 0.25, the uniformity of SERR wide-wise distribution could be ignored [13] but Gong et al. [7] showed that it is not sufficient to assure a uniform G_I wide-wise distribution. The numerical results and analysis [7-9, 15] demonstrated that the non-uniformity ratio β is related to the stacking sequence, the stiffness ratio parameter D_c and geometrical parameter including specimen width b, specimen thickness h, and initial crack length a_0. Besides crack length, Jiang et al. [16-17] studied the impact of the number of plies n, the thickness of adhesive layer h_e, and the elastic modulus of adhesive layer E_e on the non-uniformity ratio $\beta = G_{Imax}/G_{Iavg}$. It was concluded that the non-uniformity ratio β is related to the number of plies and the effects of h_e and E_e on β can be neglected. Shahani [18] investigated the effect of ligament length on

the strain energy release rate of MD DCB specimen and found that ligament length affects the energy release rate if it is less than twice the thickness of the specimen. M.M.Shokrieh et al. also found that D_c has significant effect on R-curve and steady-state propagation toughness [19] and the initial delamination length has a slight effect on the the shape of bridging law and energy dissipation [20]. Their work indicated that the non-uniformity ratio β can vary widely as a function of stacking sequence, specimen width, specimen thickness, and materials properties for composite laminates. Focusing on the effects of DCB test parameters on the measured fracture toughness of MD laminate, the studies mentioned above have only concerned the stacking sequence and the geometrical parameters including specimen width, specimen thickness, and initial crack length. However, the effects of material properties including the Poisson's ratio v_{12}, the elastic modulus E_{11}, E_{22}, and shear modulus G_{13} on the non-uniformity ratio β have not been analyzed independently. Besides, comparing the analysis of effects of the DCB geometrical parameter on non-uniformity ratio β, less attention has been paid to the determination of the non-uniformity ratio β.

Some empirical and practical methods for evaluating the critical energy release rate and the non-uniformity ratio β were proposed as well. Based on 1D Euler–Bernoulli theory and Winkler foundation, a detailed model was proposed to obtain the energy release rate of the symmetric DCB specimen [21]. Based on the complementary energy of a laminated beam including hydrothermal effects, De Gracia et al. [22] proposed an analytical method for calculating G_{IC} of symmetric $[(\pm 45°)_4]_{sym}$ and anti-symmetric $[(\pm 45°)_4]_{anti\text{-}sym}$ laminates. Shokrieh et al. [8-9] mentioned a list of parameters which may affect the distribution of pure mode I SERR of MD DCB specimens and indicated that the value of β can be guessed from the database by carrying out a huge amount of computational cases. Jiang et al. [23] proposed a practical formula for β as a function of the geometrical parameters a/b, and number of plies n, but lots of fitting parameters were required. Theoretical solutions for the SERR non-uniformity ratio β were also proposed. Based on a sixth-order beam theory, M.M.Shokrieh et al theoretical approach is presented to calculate the mode I interlaminar fracture toughness [24, 25]. An equivalent plate model based on Kirchhoff theory was presented by Jiang et al. [26] for determining non-uniformity ratio β. In their work, a

simplified plate model based on Kirchhoff theory and virtual crack closure technique (VCCT) has been provided to estimate the SERR distribution shape and the non-uniformity ratio β for the un-symmetrical DCB specimens. In order to measure correctly pure mode I fracture toughness of a MD laminate using DCB tests by integrating the ratio β, a fast and simple method to evaluate the SERR non-uniformity ratio β is essential and necessary in engineering applications.

In this work, the main objective is to investigate which composite laminate parameters affect the SERR non-uniformity ratio β and furthermore, to propose a novel closed-form expression to determine the real pure mode I fracture toughness measured using MD DCB specimens. The analysis was based on numerical modeling of MD DCB specimen. Firstly, the non-uniform distribution of SERR in term of β was introduced. Then, a finite element modeling using virtual crack closure technique (VCCT) was described and the accuracy and mesh convergence of this numerical model were validated by comparing with the experimental results of the reference [27]. Secondly, in order to get the parameters affecting the width-wise distribution of G_I at the crack front, several cases were investigated numerically by varying material elastic constants, stacking sequences, widths, and thicknesses of MD DCB specimens. Finally, a semi-empirical closed-form expression has been proposed to estimate the non-uniformity ratio β and validated with numerical results.

2.Non-uniformity ratio β and Numerical models

2.1.Non-uniformity ratio β

A typical distribution of interlaminar fracture toughness along the crack front of UD and MD DCB specimens is shown in Figure 1, the specimen is made by T800/X850, having initial crack length a_0 = 40 mm, width b = 15 mm. Their schematic diagrams of corresponding curved crack front after crack propagation are given as well. It can be clearly seen that the G_I/G_{Iavg} is not uniform along the normalized width of the specimen; it has a maximum in the middle of the specimen and decreases as the crack front approaches the edges of specimen. Thus, the central area reaches the critical strain energy release rate firstly, which causes an

obviously curved or thumbnail shape crack front in MD DCB specimen during the crack propagation, as shown in Figure 1.

A non-uniformity ratio β is defined to evaluate the level of non-uniform distribution of SERR along the crack front, expressed as follows:

$$\beta = \frac{G_{Imax}}{G_{Iavg}}\% = \text{maximum}\left(\frac{G_I}{G_{Iavg}}\right)\% \quad (1)$$

According to previous research of [7-9], it is reported that non-uniformity ratio β is associated with coupling parameter D_c, geometrical parameters a_0, h and b, and material properties. Thus, it can be defined a function as follows:

$$\beta = f(D_c, a_0, b, h, E_i) \quad (2)$$

Where, a_0 is the initial crack length; b is the specimen width; h is the specimen thickness; and E_i refers to the materials properties.

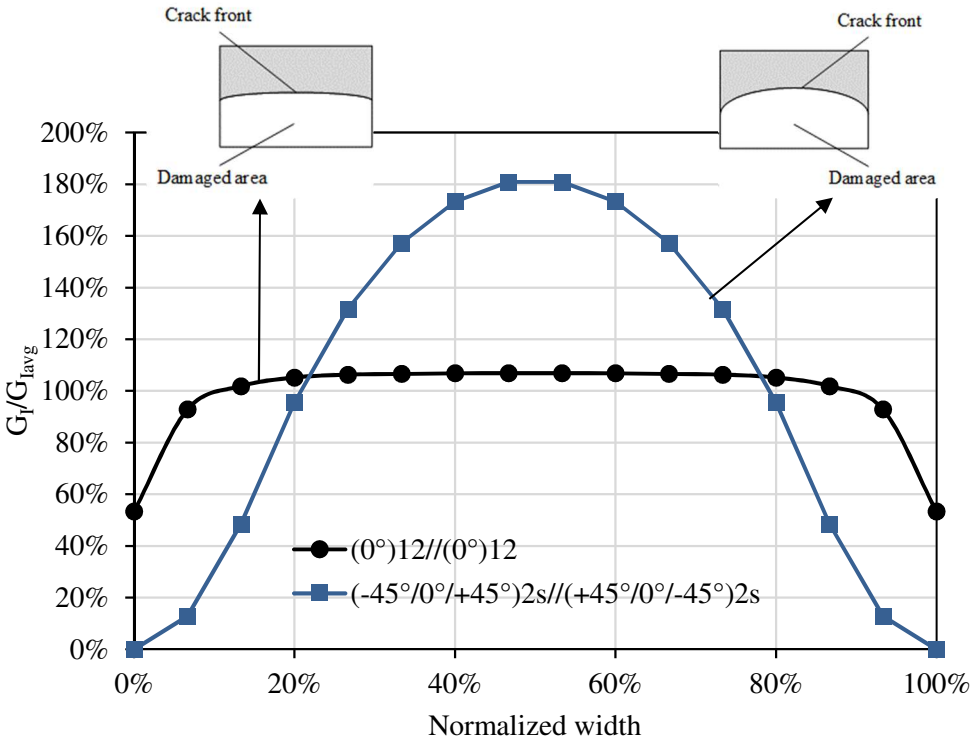

Figure 1 A typical non-uniform distribution of interlaminar fracture toughness on crack front and schematic diagram of corresponding curved crack front after crack propagation

2.2. VCCT and Numerical model

The VCCT is a numerical analysis method for a variety of crack propagation analysis. The method is founded on the Irwin's crack closure integral with the assumption that the energy needed to separate two surfaces is the same as the energy needed to close the same surfaces [28] and used for computing the SERR of DCB specimen. This technique has been implemented into the large commercial general finite element software Abaqus, ANSYS, and Nastran, etc. In this work, all numerical simulations have been carried out by the commercial FEM software Abaqus.

Figure 2(a) shows a typical 3D finite element model of the DCB specimen which is parallelepipedic with a dimension of 180 mm (L) × 25 mm (b) × 2.96 mm ($2h$). The thickness of each layer of elements is 0.185 mm. In the following sections and computational cases, some geometric dimensions are different above and notified. Referring to the test standard ASTM 5528, the boundary condition of DCB specimen and mesh are displayed in Figure 2(b). A displacement loading is applied at the upper beam while the freedom U3 at the lower beam is constrained. In this model, 4 elements are divided along the thickness for each arm. And along the width of specimen, 15-20 elements are divided. Since the VCCT method is sensitive to the element size, the mesh close to the crack front was locally refined to guarantee a good accuracy of the results, as shown in Figure 2(b). In order to get the appropriate mesh refinement and computational efficiency, some DCB specimens with different length size close to the crack front are performed. By carrying out cases with different element sizes, it can be concluded that when the element size is less than 2 mm, the mesh convergence can be obtained. Thus, the element size close to the crack front is taken as 0.5 mm in the numerical study. The parameters in VCCT numerical models refers to the Ref [29]. To validate the effectiveness and accuracy of the numerical model, and a DCB numerical test was carried out and compared with the results from [27, 29]. Figure 2 (c) shows the comparison of load-displacement curves of MD DCB specimens with a lay-up $(-45°/0°/+45°)_{2s}//(+45°/0°/-45°)_{2s}$, and a geometry of 180 mm × 25 mm × 2.96 mm, a_0 = 40 mm, using material T800/X850. Good agreements in stiffness between the numerical results and experimental results in literature have been obtained. These numerical models

with different specimen parameters will be carried out in next section.

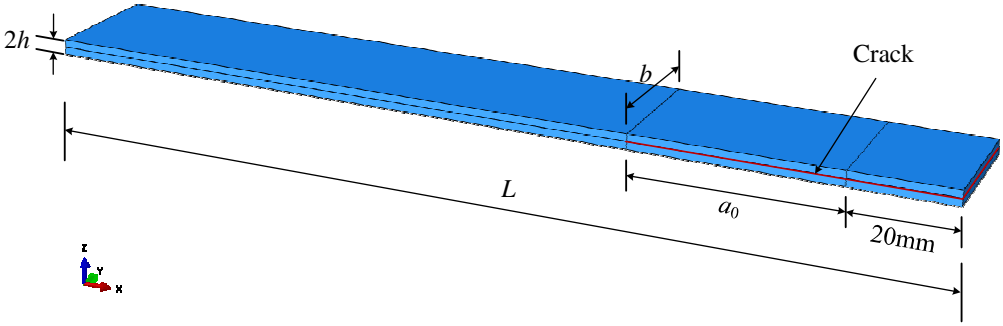

(a)

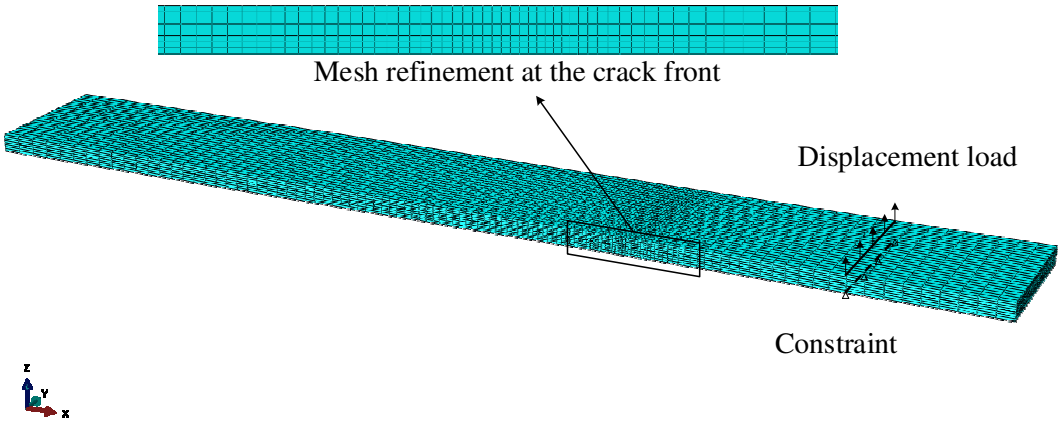

(b)

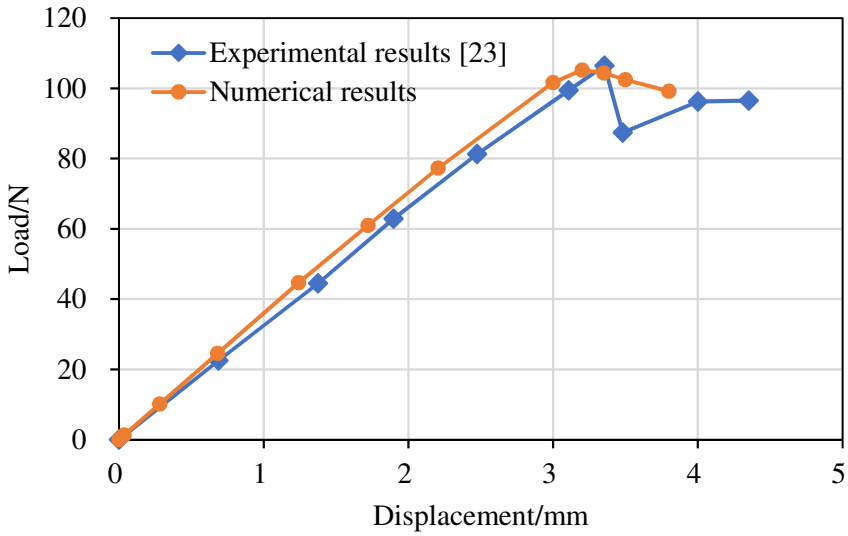

(c)

Figure 2 (a) Dimension of DCB specimen; (b) Mesh and boundary condition of DCB test; (c) Comparison of load-displacement curves of MD DCB specimens

3.Computational cases and discussion

3.1.Computational cases

Numerical calculations have been carried out on the MD DCB specimens with different composites materials stacking sequences, and a wide range of thickness h, width b, and material parameters. To reduce the numbers of parameters, the specimen initial crack length a_0 was fixed to 40 mm in this study.

In order to independently investigate the influence of materials constants, six different composite materials, T800/X850 [27], T300/9770, glass/epoxy, fabric material, IM7/8552 [9], and AS4/PEEK [9], have been modeled. Their elastic properties, referred as material constants in this paper, are listed in Table 1.

Table 1 Mechanical elastic properties of six materials

	Material	E_{11}	$E_{22}=E_{33}$	$G_{12}=G_{13}$	G_{23}	$\nu_{12}=\nu_{13}$	ν_{23}	E_{11}/E_{22}
		GPa						
M-1	T800/ X850	195	8.58	4.57	2.9	0.33	0.48	22.72
M-2	T300/ 9770	150	11	6	3.7	0.25	0.45	13.63
M-3	Glass/Epoxy	36.2	10.6	7.2	2.6	0.26	0.48	3.42
M-4	Balanced Fabric Glass/Epoxy	18.6	18.6	3.19	2.42	0.175	0.372	1.00
M-5	IM7/8552	160	10	4.8	3.2	0.31	0.52	16
M-6	AS4/PEEK	138	10.5	6.3	3.5	0.3	0.5	13.14

Three series of stacking sequences, A-1, A-2, A-3 are designed, as shown in Table 2, and each series of stacking sequences has seven ply angles α (0°, 15°, 30°, 45°, 60°, 75°, 90°). All the designed lay-ups of MD DCB specimens meet following conditions:

$$A_{16}=A_{26}=B_{ij}=D_{16}=D_{26}=0$$

Where, A_{16}, A_{26}, B_{ij}, D_{16}, and D_{26} are the coupled terms in stiffness matrix of MD DCB laminates. Recall that $\boldsymbol{A}$ is the stiffness matrix; $\boldsymbol{B}$ is the coupling stiffness matrix; $\boldsymbol{D}$ is the bending stiffness matrix. Thus, uncoupled MD laminates are obtained, and these laminates have the same stiffness properties in bending and in tension like homogenous material.

Table 2 Stacking sequence of designed specimens

	Numbers of plies	Lay-ups	α
A-1 (α)	16-ply	$[\alpha/-\alpha_2/\alpha/-\alpha/\alpha_2/-\alpha]_{sym}$	0°, 15°, 30°, 45°,60°,75°,90°
A-2 (α)	12-ply	$[\alpha/-\alpha/0/-\alpha/\alpha/0]_{anti\text{-}sym}$	
A-3 (α)	12-ply	$[\alpha/0/-\alpha/-\alpha/0/\alpha]_{anti\text{-}sym}$	

To investigate the influence of the stacking sequence, specimen width, materials, and thickness on the non-uniformity ratio β, several series of computational cases are considered. The modeled DCB specimens with three different lay-ups, 8 different thicknesses, 8 different widths, and 6 different materials, are summarized in Table 3.

In Table 3, computational series (1) is designed for investigation on the effect of specimen thickness on β. Same material T800/ X850 (M-1), stacking sequence A-1(0°), and specimen width b are designed for each case. 7 values are considered for the specimen thickness h^*: 0.74, 1.11, 1.48, 2.22, 2.96, 4.44, 8.88, and 17.76;

Computational series (2) is designed mainly for investigation on the effect of specimen width b on β. Same material T800/ X850 (M-1), stacking sequence A-1(α), and specimen thickness are designed for these cases. 8 values are considered for specimen width b^*: 7.5, 15, 20, 25, 30, 35, 50, and 100. α takes 7 values: 0°, 15°, 30°, 45°, 60°, 75°, and 90° so that the variation of non-uniformity ratio β versus to the coupling parameter D_c can be obtained;

The combination of computational series (2) and some of series (3) is designed for investigation on the effect of specimen lay-ups on β. Same material T800/ X850 (M-1), specimen width b = 15 mm, and specimen thickness h = 1.48 mm are designed for these cases. In these computational series, 3 series of stacking sequences, A-1, A-2, and A-3 with different 7 values of α, are used;

Computational series (4) is designed mainly for investigation on the effect of elastic constant of material on β. Same stacking sequence A-1(α), specimen width b, and specimen thickness h are designed for these cases. M-i, with i = 1, 2, 3, 4, 5, and 6, refers to six different materials, as shown in Table 3, which include carbon fiber, glass fiber, and fabric material. α takes 7 values: 0°, 15°, 30°, 45°, 60°, 75°, and 90° as well. In order to reduce the computational time, parametric modeling and automatic post-processing based on Python script were established.

Table 3 Computational cases with different lay-ups, thicknesses, widths, and materials

Computational Series	Lay-up	Thickness (mm)	Width (mm)	Materials	Numbers of cases
(1)	A-1(0°)	h^*	25	M-1	8
(2)	A-1(α)	1.48	b^*	M-1	56
(3)	A-2(α) A-3(α)	1.48	15	M-1	14
(4)	A-1(α)	1.48	15	M-*i*	42

The computational series (5)-(8), as shown in Table 4, are used to comprehensively reveal the effect of the Poisson's ratio v_{12}, the elastic modulus E_{11}, E_{22}, and shear modulus G_{13} on the non-uniformity β independently. Here, the shear modulus out of plane plays a role in mode-I delamination so that shear modulus G_{13} instead of G_{12} is used. The geometry of the specimen is h = 1.48 mm, b = 25 mm, and a_0 = 40 mm, using lay-up of A-1(30°). Based on the material property of M-1(T800/X850), different parameters of E_{11}, E_{22}, G_{13}, and v_{12} are chosen as following. Here, E_{11}^* can take 9 values: 10, 20, 35, 50, 100, 150, 195, 250, and 500; E_{22}^* can take 6 values: 1, 8.58, 20, 50, 100, and 195; G_{13}^* takes 6 values: 1, 4.57, 10, 20, 30, and 50; v_{12}^* takes 7 values: 0.11, 0.22, 0.33, 0.44, 0.55, 0,66, and 0.77, as shown in computational (5) - (8) respectively.

Table 4 Computational cases of material properties with lay-up A-1(30°), and h = 1.48 mm, b = 25 mm, and a_0 = 40 mm

Computational Series	E_{11} (GPa)	E_{22} (GPa)	G_{13} (GPa)	v_{12}	Number of cases
(5)	E_{11}^*	8.58	4.57	0.33	9
(6)	195	E_{22}^*	4.57	0.33	6
(7)	195	8.58	G_{13}^*	0.33	6
(8)	195	8.58	4.57	v_{12}^*	7

3.2.Results and discussion

In this section, the effects of the studied parameters of MD DCB specimens on non-uniformity β are discussed and analyzed.

3.2.1.Effect of specimen thickness on β

Numerical results of computational series (1) are shown in Figure 3. It shows the non-uniformity ratio β for different width/thickness ratio with 8 different thicknesses. Here, the b/h ratio increases from 1.4 to 33.8 while the parameters including the width b, the crack length a_0, and the ply orientation α are kept constant. It can be seen that the non-uniformity ratio β of the unidirectional specimen decreases from 117% to 105%. When b/h ratio exceeds 5, the β value has a very slow decline, and gradually reaches a nearly constant value (105%). The b/h ratio for thin plate usually exceeds 10. Therefore, most of the DCB specimens can be regarded as thin-plates and the effect of specimen thickness on β can be ignored. Similar conclusions can be found in Ref [30].

Thus, β is a function of only the initial crack length a_0, the specimen width b, and the materials properties E_i when b/h ratio exceeds approximately 5 and its expression can be simplified from Eq. 2 to the following:

$$\beta = f(D_c, b, E_i) \quad (3)$$

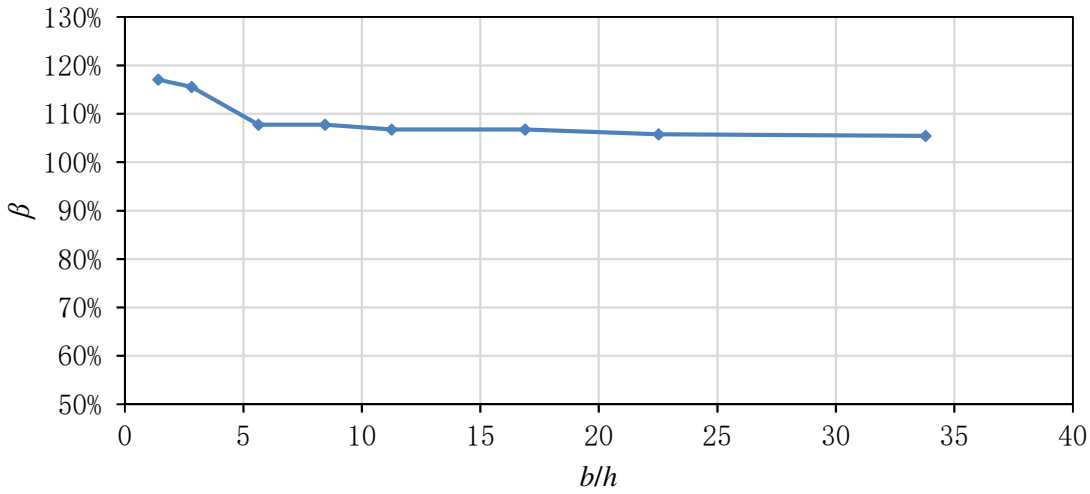

Figure 3 Variation of non-uniformity ratio β versus to b/h ratio for DCB specimens

3.2.2.Effect of specimen width on β

Numerical results of computational series (2) are shown in Table 5. The calculation is performed on material T800/ X850 (M-1) having b = 15 mm, h = 1.48 mm, and the stacking sequence $[\alpha/-\alpha/\alpha_2/-\alpha/\alpha_2/\alpha]_{sym}$ with α varying from 0° to 90°. It can be found that the non-uniformity ratio β corresponding to α = 45° reaches the top when the specimen width b is

less than 15 mm, or b/h ratio is less than 10. Figure 4(a) shows a part of results in Table 5, it can be clearly seen that the specimen width has remarkable influence on the non-uniformity ratio β. For a given initial crack length and coupling parameter D_c, the G_I distribution becomes more uniform as the specimen width b increases. The similar results can be found in the reference [7, 9]. Figure 4(b) shows a variation of non-uniformity ratio β versus to the specimen width from [7, 9]. It can be seen that β of specimen with a smaller width is much higher than that of specimen with a larger width, which shows similarly an exponential relationship.

Table 5 Numerical results of β obtained from computational series (2) with h = 1.48 mm

A-1 α	D_c	Specimen width (mm)							
		7.5	15	20	25	30	35	50	100
0°	0.0048	115%	110%	107%	106%	105%	104%	104%	104%
15°	0.1174	146%	133%	124%	118%	115%	114%	114%	115%
30°	0.5415	182%	161%	146%	134%	127%	123%	119%	116%
45°	0.7056	192%	181%	168%	156%	145%	136%	124%	117%
60°	0.5415	173%	177%	172%	164%	157%	149%	136%	119%
75°	0.1174	133%	142%	140%	138%	136%	133%	129%	116%
90°	0.0048	107%	110%	110%	109%	109%	109%	108%	105%

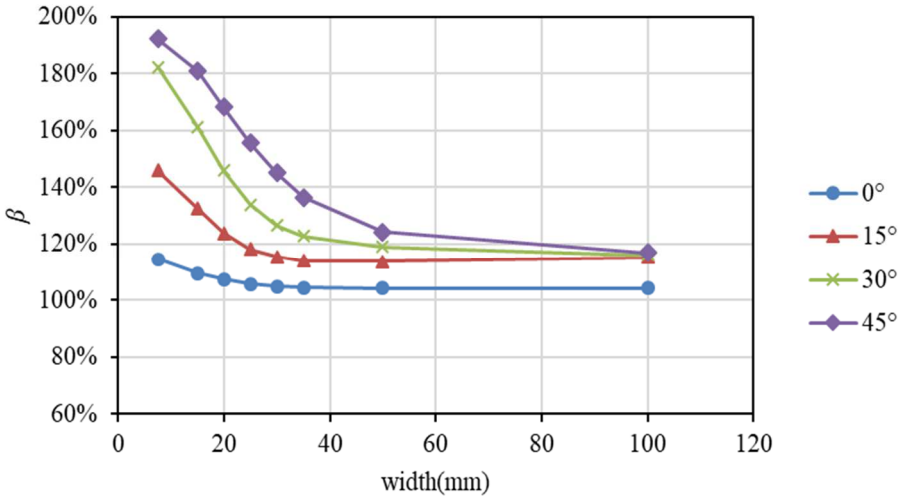

(a)

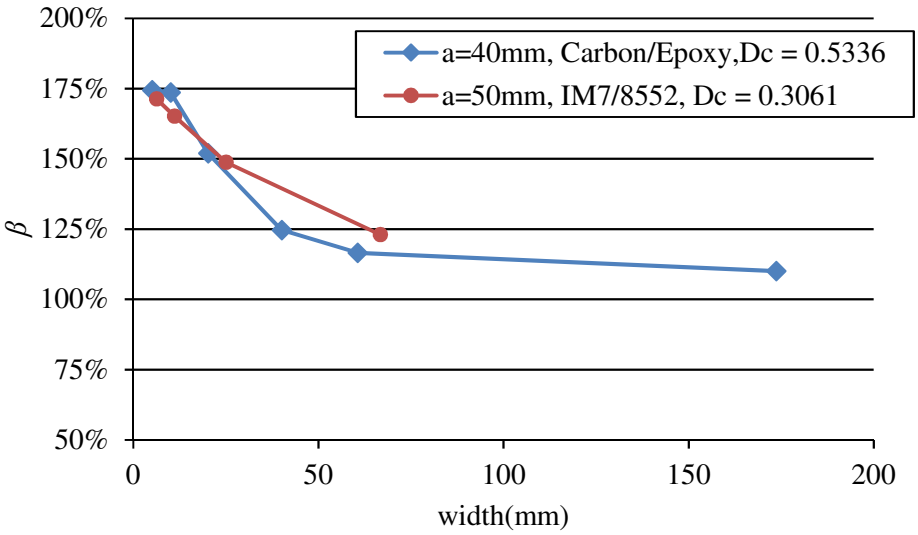

(b)

Figure 4 (a) variation of the non-uniformity ratio β versus the specimen width from computational series (2); (b) variation of the non-uniformity ratio β versus the specimen width from reference [7, 9]

Figure 5 shows the distribution along the specimen width when $\alpha = 30°$ from A-1 (30°). It can be seen that increasing the specimen width can lead to a more uniform width-wise distribution of G_I. Especially G_I becomes nearly constant in the central part of specimen. The greater width b is, the more important the central area of constant G_I.

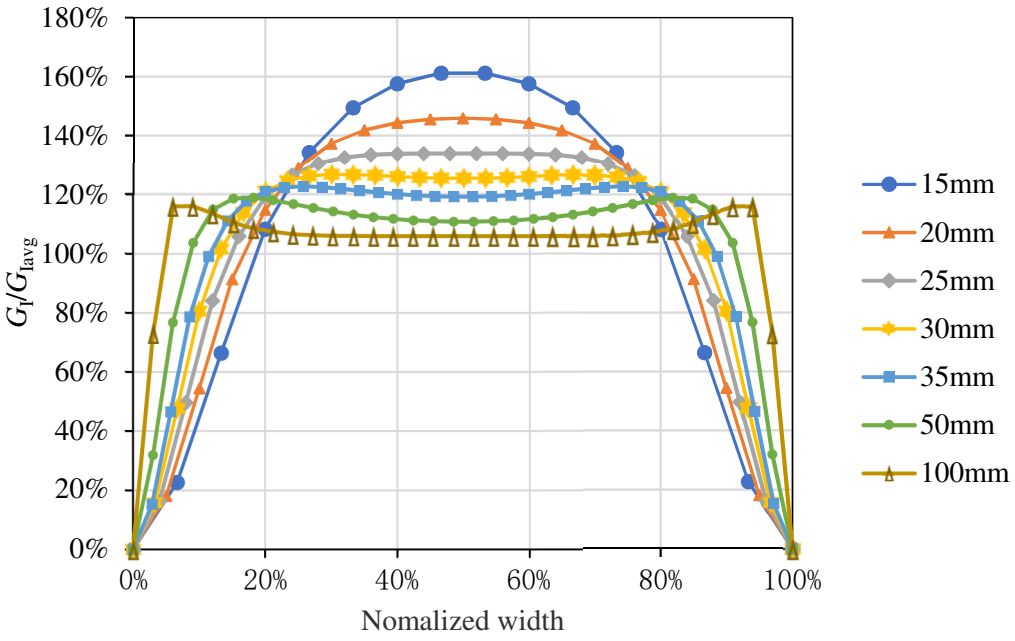

Figure 5 Width-wise distribution of G_I/G_{Iavg} of MD DCB specimen with different normalized widths b from T800/ X850 (M-1) having the stacking sequence $[\alpha/-\alpha_2/\alpha/-\alpha/\alpha_2/-\alpha]_{sym}$ with $\alpha = 30°$ and $h = 1.48$ mm

3.2.3.Effect of lay-ups on β

Figure 6 shows the width-wise distribution of G_I/G_{Iavg} of MD DCB specimen using the material T800/ X850 (M-1) with $b = 15$ mm, $h = 1.48$ mm and the stacking sequence $[\alpha/-\alpha/\alpha_2/-\alpha/\alpha_2/\alpha]_{sym}$, where the fiber orientation α varies from 0° to 90°. Remarkable effect of β on the distribution can be observed. G_I/G_{Iavg} is not uniform along the specimen width whatever the ply-angle α is. It has a maximum in the middle of the width and subsequently decreases as the crack front approaches the edges. The G_I/G_{Iavg} with $\alpha = 45°$ reaches the maximum value, compared with other fiber orientation angle, as shown in Figure 6. Figure 7 shows the variation of non-uniformity β of SERR in MD DCB specimens as a function of D_c for three lay-ups using the material T800/X850 (M-1). It can be clearly seen that whatever the lay-up is, the non-uniformity β shows a same evolution trend with respect to D_c.

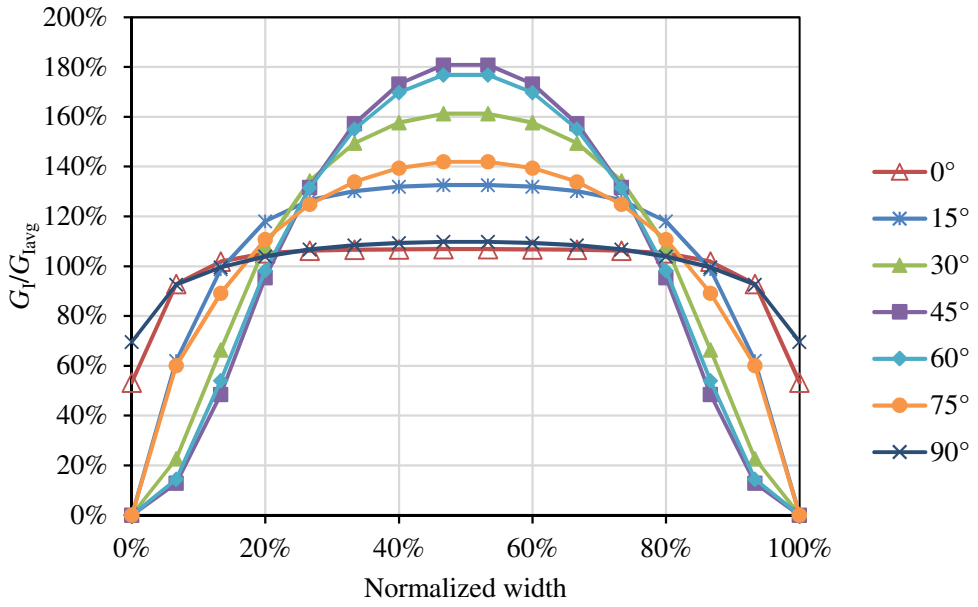

Figure 6 Width-wise distribution of G_I/G_{Iavg} of MD DCB specimen with different fiber orientation angle α from T800/X850 (M-1) having the stacking sequence $[\alpha/-\alpha_2/\alpha/-\alpha/\alpha_2/-\alpha]_{sym}$ with b = 15 mm, h = 1.48 mm

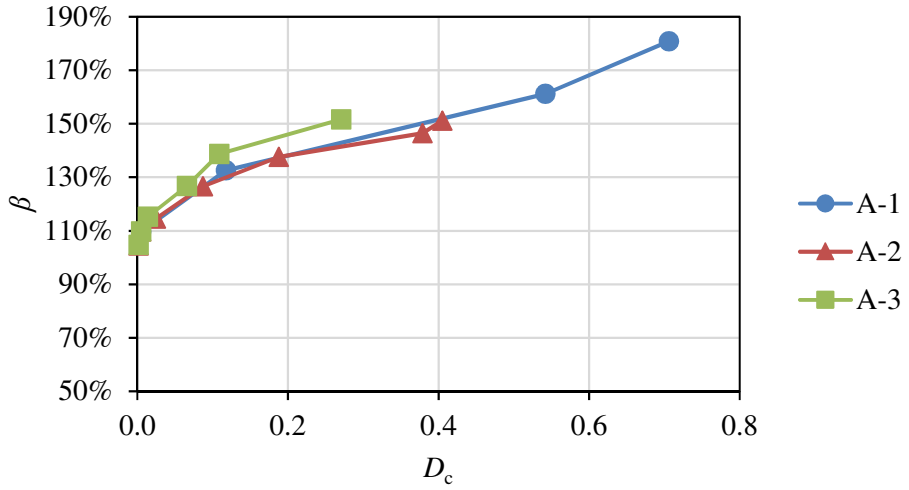

Figure 7 Variation of non-uniformity ratio β in MD DCB specimens as a function of D_c for three lay-ups: A-1 $[\alpha/-\alpha_2/\alpha/-\alpha/\alpha_2/-\alpha]_{sym}$, A-2 $[\alpha/-\alpha/0/-\alpha/\alpha/0]_{anti\text{-}sym}$, and A-3 $[\alpha/0/-\alpha/-\alpha/0/\alpha]_{anti\text{-}sym}$ using the material T800/X850 (M-1)

3.2.4.Effect of elastic constants of material on β

Numerical results of computational series (4) are shown in Table 6. Figure 8 illustrates the comparison of (β - β_0) versus (D_c-D_{c0}) obtained from MD DCB specimen having the lay-up

A-1 $[\alpha/-\alpha_2/\alpha/-\alpha/\alpha_2/-\alpha]_{sym}$ with different materials M-1 and M-3. It can be seen that the level of anisotropy in term of $\eta = E_{11}/E_{22}$ of different materials has an obvious effect on the non-uniformity ratio β. For a given (D_c - D_{c0}), the higher the value of the ratio η, the greater the value of (β - β_0). The similar results can be found in the reference [7]. Figure 9 shows a variation of non-uniformity ratio β as a function of coupling parameter D_c for three materials [7]: G/E (Glass/Epoxy balanced fabric), C/E (Carbon/Epoxy quasi-UD sheet), and C/E (Carbon/Epoxy -UD sheet). It can be seen that the non-uniformity ratio β seems to increase linearly as the coupling parameter D_c increases. Furthermore, for different materials, the non-uniformity ratio β is different for the same D_c.

Thus, it can be concluded that the elastic constants, especially the level of anisotropy of the materials plays also a key role in the determination of the non-uniformity ratio β. Furthermore, for different materials, all the β vs D_c curves show a similar linear relationship as well in the range of $D_c > 0.1$, as shown in Figure 7, Figure 8, and Figure 9. In addition, it can be seen that there is a small difference between the values of non-uniformity ratio β with the same D_c and the same material.

Table 6 Numerical results of computational series (4) b = 15 mm, h = 1.48 mm

Materials		Lay-up A-1 $[\alpha/-\alpha_2/\alpha/-\alpha/\alpha_2/-\alpha]_{sym}$						
		0°	15°	30°	45°	60°	75°	90°
M-1	D_c	0.0048	0.1174	0.5415	0.7056	0.5415	0.1174	0.0048
	β	110%	133%	161%	181%	177%	142%	110%
M-2	D_c	0.0046	0.0752	0.3941	0.5611	0.3941	0.0752	0.0046
	β	110%	130%	155%	173%	168%	137%	110%
M-3	D_c	0.0198	0.0425	0.1163	0.1671	0.1163	0.0425	0.0198
	β	119%	123%	132%	136%	134%	126%	121%
M-4	D_c	0.0305	0.0634	0.1947	0.3128	0.1947	0.0634	0.0305
	β	125%	134%	150%	159%	150%	134%	125%
M-5	D_c	0,0060	0,0951	0,4707	0,6473	0,4707	0,0951	0,0060
	β	111%	132%	159%	177%	173%	140%	111%
M-6	D_c	0,0068	0,0766	0,3675	0,5208	0,3675	0,0766	0,0068
	β	111%	130%	154%	171%	167%	138%	113%

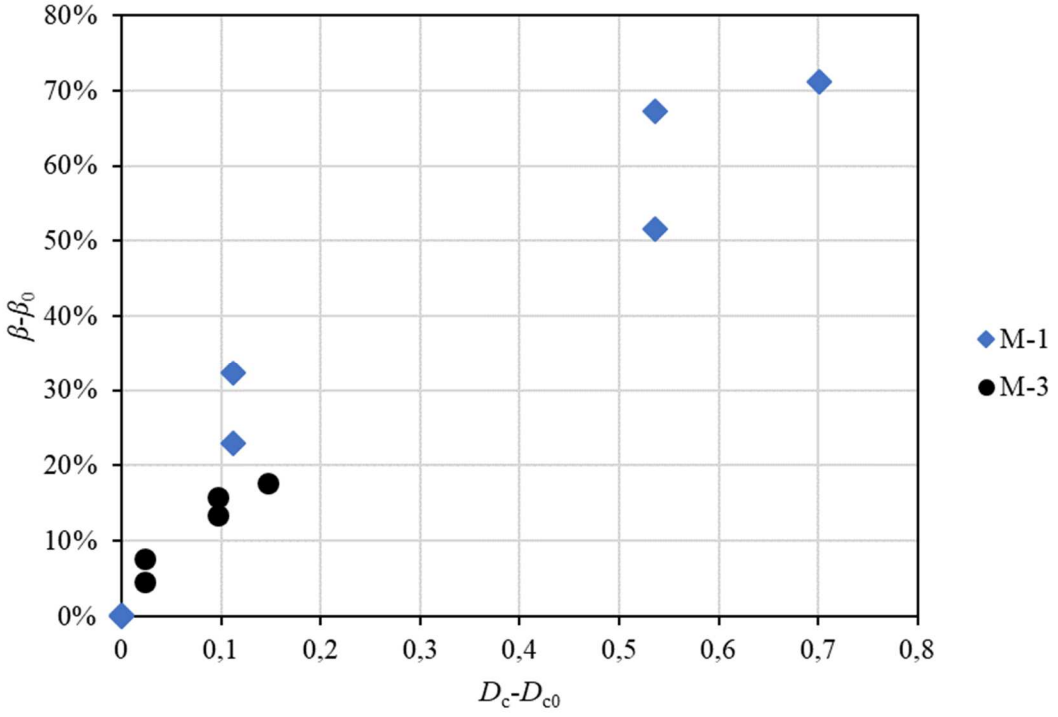

Figure 8 Comparison of the (β - β_0) versus (D_c-D_{c0}) curves using different materials (UD laminates, b = 15 mm, h = 1.48 mm)

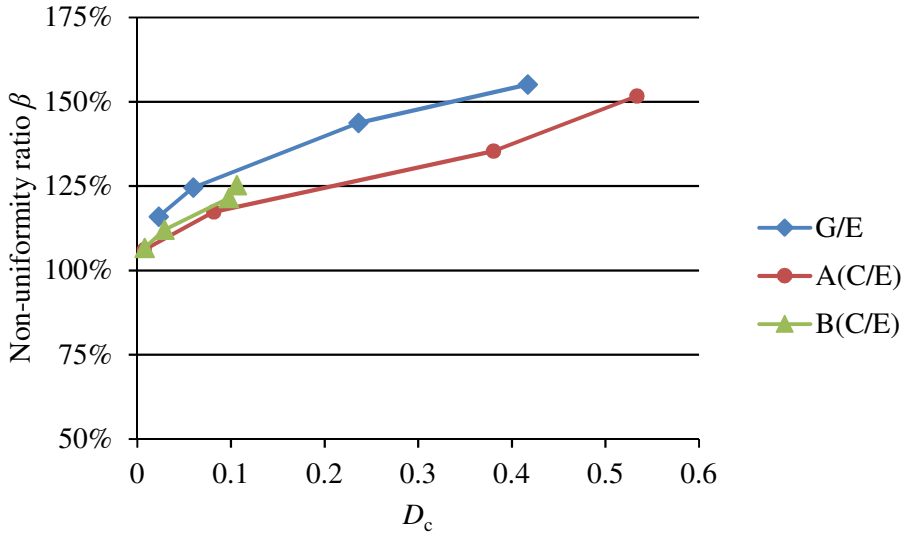

Figure 9 Variation of the non-uniformity ratio β as a function of D_c [7]

3.2.5. Effect of each elastic constant of ν_{12}, E_{11}, E_{22}, and G_{13} on β

The computational series (5)-(8) are designed to understand the impact of some elastic constants of the material on the non-uniformity ratio β. They consist in varying only one of

elastic constants among Poisson's ratio v_{12}, elastic modulus E_{11}, E_{22}, and shear modulus G_{13} and to keep all other elastic constants of M-1 material unchanged. Herein the lay-up is A-1 $[\alpha/-\alpha/\alpha_2/-\alpha/\alpha_2/\alpha]_{sym}$ with the geometry of the specimen a_0 = 40 mm, b = 25 mm, and h = 1.48 mm.

From Figure 10(a), it can be seen that as v_{12} increases from 0.11 to 0.77, the non-uniformity ratio β changes only around 4%. Figure 10(b) shows the influence of E_{11} on the non-uniformity ratio β. It shows that β increases rapidly from 121% to 130% as E_{11} is less than about 50 GPa, and subsequently has a slow increasing trend after that. Figure 10(c) shows that the non-uniformity β varies from 131% to 164% as E_{22} increases from 1 GPa to 195 GPa. From Figure 10(d), we can see that the non-uniformity β varies from 141% to 103% as G_{13} increases from 1 GPa to 50 GPa.

According to the results shown in Figure 10 (a)-(d), it can be concluded that the effect of parameters E_{11}, E_{22}, and G_{13} are much stronger than that of Poisson's ratio v_{12}, so the influence of Poisson's coefficient v_{12} can be negligible. Moreover, the non-uniformity ratio β increases as the values of E_{11} and E_{22} increase. On the contrary, β decreases with the increase of G_{13}.

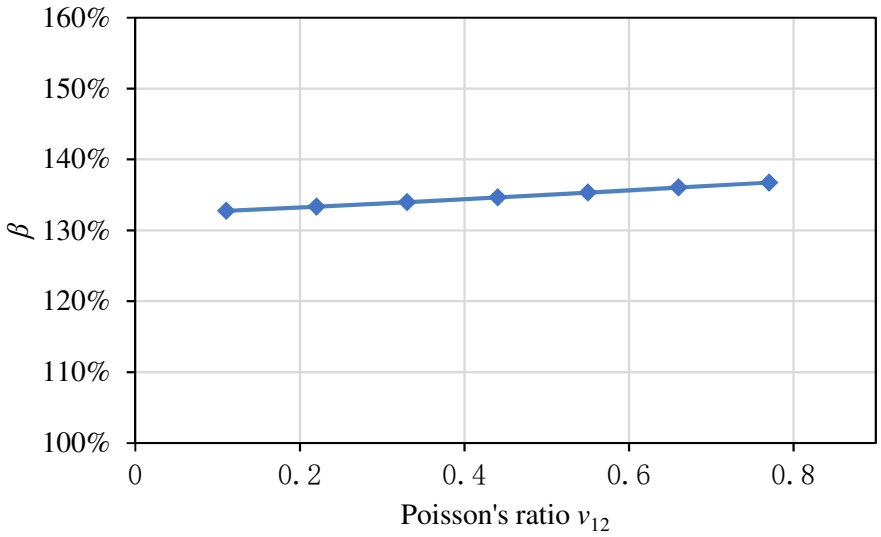

(a) β vs. v_{12}

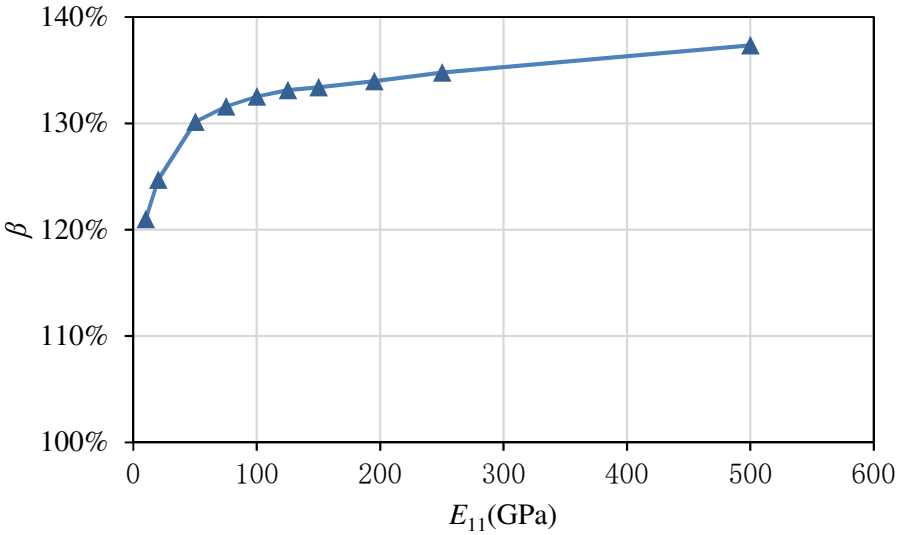

(b) β vs. E_{11}

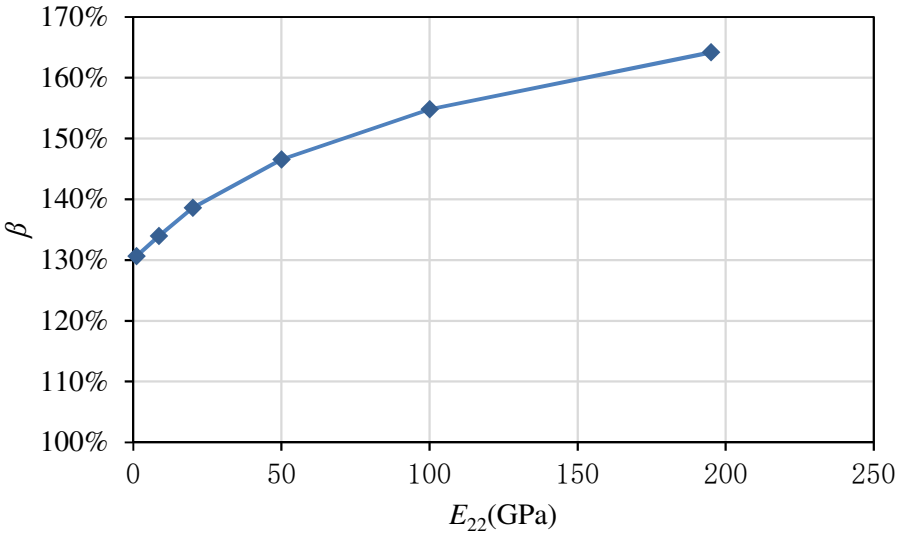

(c) β vs. E_{22}

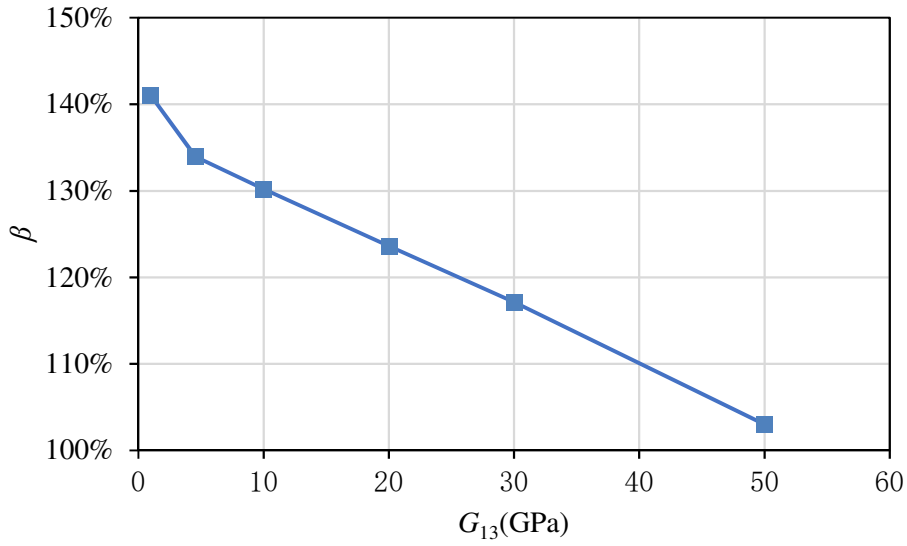

(d) β vs. G_{13}

Figure 10 Variation of non-uniformity ratio β with respect to the elastic constants of unidirectional laminate: v_{12}, E_{11}, E_{22}, and G_{13}

4.Proposition of close-form expressions for determination of non-uniformity ratio β

In this section, based on the above analysis of the numerical results on the influence of different parameters, new semi-empirical close-form expressions are proposed for predicting the SERR distribution ratio β of any uncoupled MD DCB specimen in a large range. From Figure 7, Figure 8, and Figure 9, it can be seen that for a given material the β vs D_c curves show a similar linear relationship as well in the range of $D_c > 0.1$. And from Figure 4, an exponential relationship between β and the width of specimens can be found to define the formula with different width of MD DCB for a given material with $a_0 = 40$ mm, $b/h > 5$.

4.1.Case 1: a given geometry of the specimen: $a_0 = 40$ mm, $b = 15$ mm and $b/h > 5$

For a given geometry of a MD DCB specimen: $a_0 = 40$ mm, $b = 15$ mm, and b/h exceeding 5, the general Eq. 3 of β can be concretized as following:

$$\beta = k(D_c - D_{c0}) + \beta_0 \qquad (4)$$

Where β_0 and D_{c0} denote the value of β and the value of D_c for UD DCB specimen of the same geometry, respectively. β denotes non-uniformity ratio of a MD laminate made from the same prepreg of a UD one. Herein D_c and D_{c0} can be determined easily by classical laminate theory from in-plane elastic constants of the material and the stacking sequence of the

laminate. k is a unit-less parameter which depends only on the basic elastic properties of UD laminates. So, from Eq. 4 the parameter k can be written as:

$$k = \frac{\beta - \beta_0}{D_c - D_{c0}} = f(E_i) \qquad (5)$$

According to the analysis of the results in section 4, the effects of E_{11}, E_{22}, and G_{13} on β are stronger than other material parameters. Furthermore, the non-uniformity β increased with the increase of E_{11} and E_{22}, while β increased with the decrease of G_{13}. Thus, a new dimensionless parameter $\sqrt{\frac{E_{11}^2}{E_{22}G_{13}}}$ is proposed to investigate the relationship between k and $\sqrt{\frac{E_{11}^2}{E_{22}G_{13}}}$. If k is calculated from the numerical results of β and β_0 obtained in series (4) where 6 different materials were considered, its variation versus $\sqrt{\frac{E_{11}^2}{E_{22}G_{13}}}$ was found approximately linear, as shown in Figure 11. Thus, it can be expressed as follows:

$$k = m\left(\sqrt{\frac{E_{11}^2}{E_{22}G_{13}}}\right) + n \qquad (6)$$

Where, m and n are two constants to be determined by linear fitting the numerical results obtained. Their values for this case are m = -0.0083 and n = 1.212. So, the Eq. 4 becomes

$$\beta = \left(-0.0083\sqrt{\frac{E_{11}^2}{E_{22}G_{13}}} + 1.212\right)(D_c - D_{c0}) + \beta_0 \qquad (4A)$$

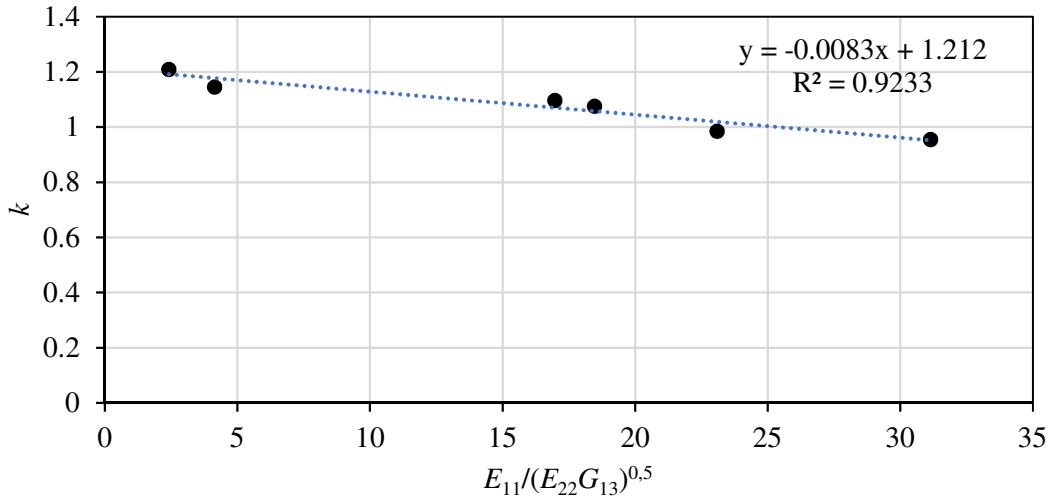

Figure 11 Linear relationship between k and $\sqrt{E_{11}^2/(E_{22}G_{13})}$

in the case of a_0 = 40 mm, b = 15 mm and b/h > 5

The application of Eq. 4A for any material and any lay-up needs not only the value of D_c and D_{c0}, but also the value of β_0. The interest of this formula is that the non-uniformity ratio β can be determined analytically without numerical model. As mentioned above, the determination

of D_c and D_{c0} is based on laminate theory so is completely analytical. However, an analytical formula for determining β_0 is not yet found as we know. The method to resolve this problem for the moment is to fit the numerical results so as to obtain the empirical law. The Figure 12 shows a linear relationship between β_0 and D_{c0} for six materials calculated in series (4). The linear fitting law can be written as:

$$\beta_0 = 5.856D_c + 1.0714 \quad (7)$$

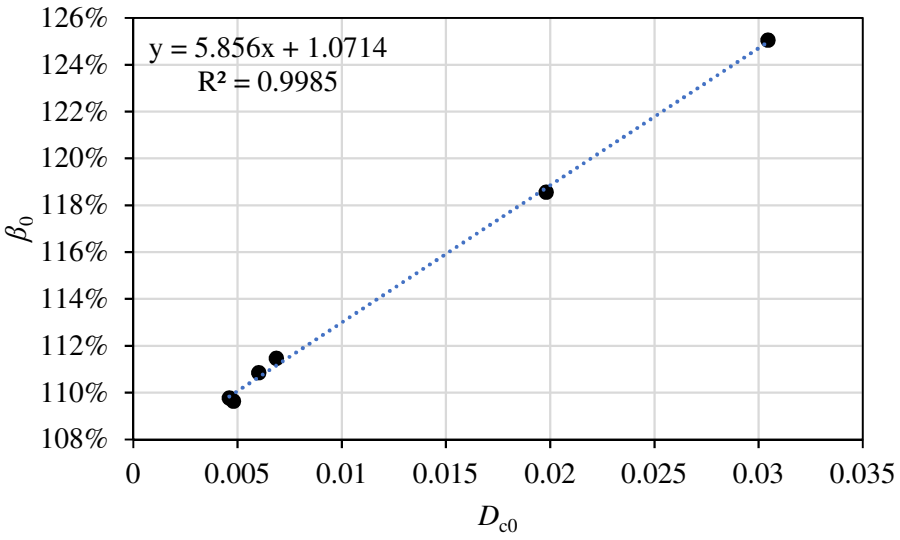

Figure 12 Linear relationship between β_0 and D_{c0} the case of a_0 = 40 mm, b = 15 mm, and $b/h > 5$

Substituting β_0 by Eq. 7 in Eq. 4A, we can obtain the following analytical expression:

$$\beta = (-0.0083\sqrt{\frac{E_{11}^2}{E_{22}G_{13}}} + 1.212)(D_c - D_{c0}) + 5.856D_c + 1.0714 \quad (4B)$$

4.2.Case 2: a given material and a_0 = 40 mm, $b/h > 5$, but another width of DCB specimen

From Figure 4, we can see that for a given material (prepreg) with a_0 = 40 mm, $b/h > 5$, the non-uniformity ratio β and the width of MD DCB specimen show an exponential relationship whatever the value of D_c is. So, a prediction of non-uniformity ratio β with any coupling parameter D_c is expressed as follows:

$$\beta = e^{-k^*b} + \beta_\infty \quad (8)$$

when $b \to \infty$, $\beta = \beta_\infty$.

Where, b is the width of specimen, k^* is a constant which can be determined by a known (b, β) obtained numerically or by Eq. 4B; β_∞ is the non-uniformity ratio when the width is infinite. It can be seen that its value is usually between 1.15 and 1.19 for most of MD laminate from Table 5. For a given material and given geometry, β_∞ of a MD DCB specimen is generally higher than that of UD one.

Once the non-uniformity ratio β is determined for a given uncoupled MD DCB specimen, it is possible to estimate its real fracture toughness G_{IC} (relative to unidirectional one) as following

$$G_{IC} = \frac{\beta}{\beta_0} G_{Iavg} \quad (9)$$

Where G_{Iavg} is the width-width average SERR at critical load corresponding to onset of delamination, it can be calculated using the same method described in the standard ASTM 5528 [6]. In fact, this proposition is general that is also validated for UD DCB one. When the laminate is unidirectional, $\beta = \beta_0$ the G_{IC} so measured comes back to that proposed by the standard ASTM 5528 [6].

4.3. Steps of the application of the proposed method

The application of this proposed method can be summarized in details as follows for measuring pure mode I toughness by MD DCB tests:

Step 1: Choice of the geometry of MD DCB specimen that has to satisfy the following conditions: $a_0 = 40$ mm and $b/h > 5$, but $b/h > 10$ is advised;

Step 2: Determination of D_{c0} as well as D_c by the classical laminate theory from in-plane elastic constants of the material and from the stacking sequence of MD DCB; then estimation of β_0 by Eq. 7: $\beta_0 = 5.856 D_{c0} + 1.0714$;

Step 3A: If the specimen width $b = 15$ mm, β can be obtained directly by Eq. 4B:

$$\beta = (-0.0083 \sqrt{\frac{E_{11}^2}{E_{22} G_{13}}} + 1.212)(D_c - D_{c0}) + 5.856 D_c + 1.0714$$

Step 3B: If the specimen width b is different from 15 mm, β obtained for $b = 15$ mm by Eq.4B (Step 3A), denoted by β_{15}, can be introduced to Eq. 9 in order to determine the constant k^*:

$$k^* = \ln\frac{\beta_{15} - \beta_\infty}{15}$$

And then β for any width of the MD specimen b (mm) can be determined by Eq. 8:

$$\beta = e^{-k^* b} + \beta_\infty$$

Herein, β_∞ of the MD DCB has to be estimated, which should be higher than that of UD one and between 1.15 and 1.19 for most of composites;

Step 4: Determination of G_{Iavg} at critical load corresponding to onset of delamination by carrying out the MD DCB tests according to the standard ASTM 5528;

Step 5: Finally, the real fracture toughness G_{IC} for an uncoupled MD DCB specimen can be obtained by Eq. 9: $G_{\text{IC}} = \frac{\beta}{\beta_0} G_{\text{Iavg}}$.

5.Verification

In order to valid the proposed formulas, some verification cases in this section are presented and discussed. The first of verification is the comparison between the numerical results and the obtained by novel formulas. The second is the comparison between the experimental results and numerical results with different fracture toughness. Last, some literature results are also used for the verification of proposed model.

5.1.Validation by numerical results

In this section, three computational cases with different materials and lay-ups are carried out to verify the novel prediction method proposed above, as shown in Table 7. A new material M-7(HS160RM) [15], shown in Table 8, and two lay-ups, A-1(α) and A-2(α), α varying from 0° to 45°, are used for verification of Eq. 4B, as shown in Computational series (9) and (10). Computational series (11) and computational series (12) with different widths are used to validate the Eq. 8.

Table 7 Computational cases for verification

Computational Series	Material	Lay-up	Width (mm)	Thickness (mm)
(9)	M-7	A-1(α)	15	1.48
(10)		A-2(α)		
(11)	M-1	A-1(α)	7.5	
			15	
			20	
(12)	M-2	A-1(α)	7.5	
			15	
			20	

Table 8 Materials property of M-7

	Material	E_{11}	$E_{22} = E_{33}$	$G_{12} = G_{13}$	G_{23}	$\nu_{12} = \nu_{13}$	ν_{23}
		GPa					
M-7	HS160RM(Carbon/ epoxy)	109	8.819	4.315	3.200	0.342	0.380

For the cases (9-10), β_0 of material M-7 evaluated by Eq. 7 is much closer to that from numerical model (1.127 and 1.133, respectively). Figure 13 compares the results of β_0 from numerical model and from the proposed closed-form expression Eq. 4B for b = 15 mm and h = 1.48 mm. Two different lay-ups were considered using material M-7: HS160RM (Carbon/epoxy). Whatever the lay-ups, a good agreement can be concluded, because the difference relative to numerical ones is no more than 8%.

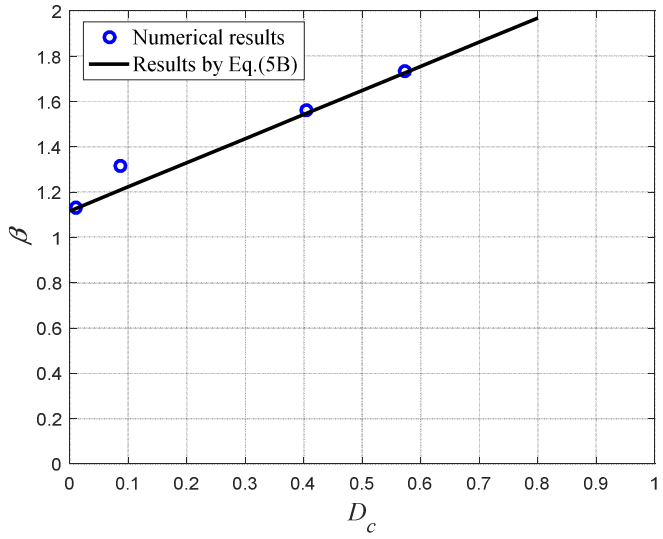

(a) Comparison of numerical results and the results from semi-empirical expression Eq. 4 for lay-up A-1 $[\alpha/-\alpha_2/\alpha/-\alpha/\alpha_2/-\alpha]_{sym}$ and materiel M-7 HS160RM (Carbon/epoxy)

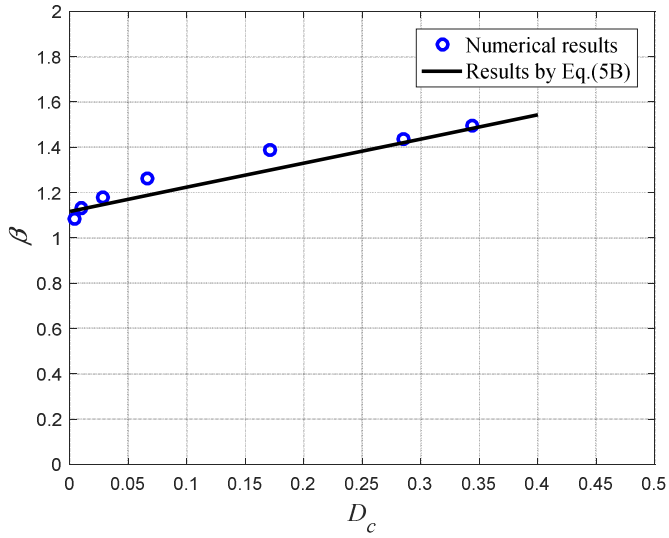

(b) lay-up A-2 $[\alpha/-\alpha/0/-\alpha/\alpha/0]_{anti\text{-}sym}$

Figure 13 Comparison of numerical results and the results from Eq. 4 with materiel M-7: HS160RM (Carbon/epoxy) and different lay-ups, h = 1.48 mm, b = 15 mm

To validate the expression 9, their results using lay-up A-1 $[\alpha/-\alpha/\alpha_2/-\alpha/\alpha_2/\alpha]_{sym}$ and two different materials with h = 1.48 mm are compared with those from numerical models in Figure 14. It can be seen that the difference of β between the numerical results and the results from Eq. 8 is small enough, especially for a specimen with usual width b, whatever the material is.

Consequently, the proposed closed-form expressions: Eq. 4B and Eq. 8 for prediction of non-uniformity ratio β are validated for most cases of MD DCB specimens.

Once the non-uniformity ratio β is determined for a given uncoupled MD DCB specimen, it is possible to estimate its real fracture toughness G_{IC} by Eq 9.

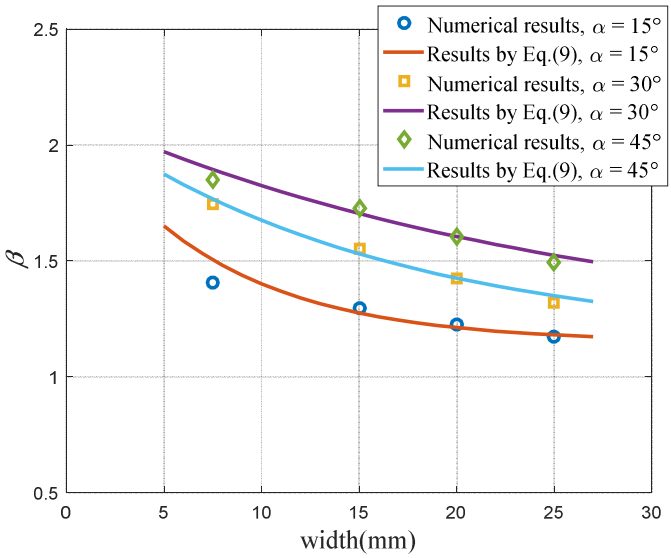

(a) M-1: T800/ X850

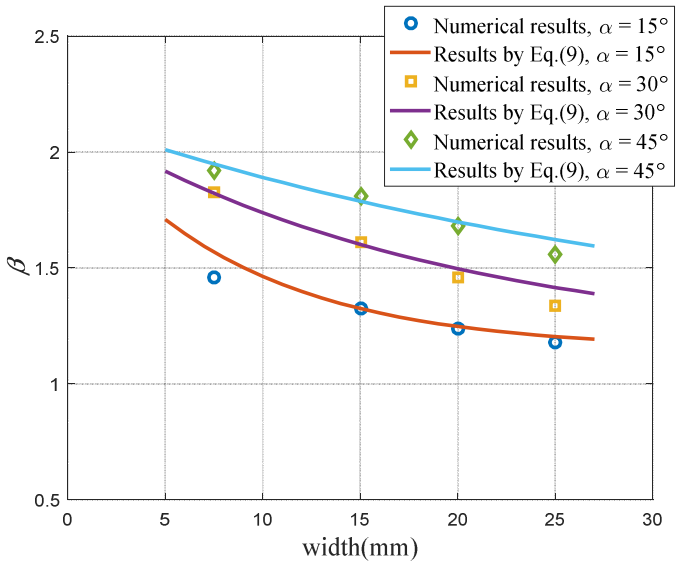

(b) M-2: T300/ 9770

Figure 14 Comparison of numerical results and the results from Eq. 7 using lay-up A-1 $[\alpha/-\alpha_2/\alpha/-\alpha/\alpha_2/-\alpha]_{sym}$ and two different materials with h = 1.48 mm

5.2. Validation by experimental results and literature results

The best experimental method to valid the proposed formula is to set a real time C-scan measurement to obtain the new surface created by the crack initiation and corresponding dissipated energy during a short time Δt. Then, the real value of G_{IC} can be calculated according to its definition. Actually, a lot of experiments in the literature have shown that the crack initiation is usually occurred in the middle of the specimen width. The line crack front in DCB specimen becomes curved crack front after crack propagation even in unidirectional specimens. This phenomenon can be accentuated in multidirectional ones. Therefore, the G_I is not constant along a line crack front, the maximal value of G_I should be in middle of the specimen width. However, these observations give neither the real value of $G_{IC,}$ nor the ratio G_{Imax}/G_{Iavg}.

Another way to valid the proposed model is to compare the results of load-displacement curves from experimental and numerical DCB tests, in which two kinds of numerical simulations are necessary. One numerical test uses the traditional fracture toughness without the correction of β, and another one uses the fracture toughness with the correction of β proposed in our model.

To further valid the novel method, experimental results from [27] are used. The configuration, geometric dimensions, and material of the specimens in [27] are the same with some computational cases in this work, as illustrated in Figure 2. The initial crack length is 40mm, the width of specimen is 25mm, the stacking sequence is $[(-45^o/0^o/+45^o)_{2s}//(+45^o/0^o/-45^o)_{2s}]$,and the material is M-1 (T800/X850). Based on the description in Section 4.3, here are the steps for modeling numerically the DCB test:

(1) β for the specimen with b = 15mm can be obtained by Eq.7 and Eq.4A, and the β value for specimen with b = 25mm is obtained by Eq.8, here, β_∞ = 1.15 is used;

(2) the real fracture toughness G_{IC} for b = 25mm can be obtained by Eq.8. Here, the fracture toughness G_{Iavg} can be obtained from load-displacement curve using simple beam theory method [31].

(3) finally two kinds of numerical model are established, one uses the average value of fracture toughness G_{Iavg}, and another model has the β correction proposed in this work.

The experimental load-displacement curve is compared with those from two numerical models in Figure 15. It can be seen that the numerical results using real toughness G_{IC} (red line) is much closer to the experimental result (blue line) than those using the average fracture toughness G_{Iavg}. Because the effect of R-curve due to fiber bridging has not been considered in our numerical models, the resistance to crack propagation after the onset of the crack is under-estimated. In conclusion, the numerical model using the real fracture toughness calculated by Eq.9 is more promising.

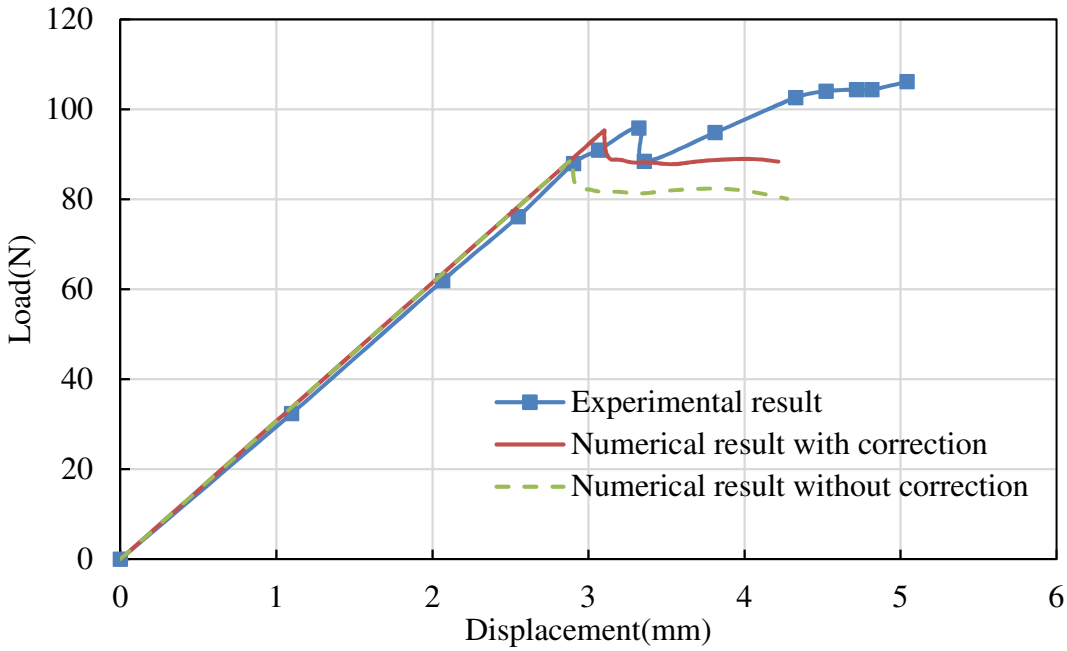

Figure 15 *Comparison of experimental load-displacement curve with those obtained by the two numerical models with or without β correction*

Some non-uniformity ratio β results from literature are presented and discussed as well. Table 9 gives the comparison of result from the proposed formulas and other results from literature using glass/epoxy materials. Here, the specimen has the same glass/epoxy material, same layups, and same geometry with a = 40mm, b = 20mm, b/h >10. According to the novel method proposed, the non-uniformity ratio β is obtained and it is quite close to other two results with maximum 5.1% error.

Table 9 Comparison of the proposed formulas with other results using glass/epoxy materials

Material	Stacking sequece	Results from Refs.		Result from Eq.4B
Glass/epoxy [7]	$[\alpha/-\alpha_2/\alpha/-\alpha/\alpha_2/-\alpha]_{sym}$ $\alpha = 30°$	1.437[7]	1.403[16]	1.386

6.Conclusion

In this study, based on numerical modeling of uncoupled multidirectional DCB specimen novel semi-empirical closed-form expressions were proposed for the determination of the width-wise non-uniformity ratio β, which is necessary to estimate the real fracture toughness of multidirectional laminates under pure mode I loading.

In the condition of initial crack length $a_0 = 40$ mm, the effect of four factors on the non-uniform width-wise distribution of SERR were investigated by numerical models of DCB specimens, including stacking sequence, specimen width, specimen thickness, and material elastic properties. Based on the analysis of the results obtained, most important conclusions can be given as follows:

1. The width-wise non-uniformity ratio β in a MD DCB specimen decreases with the increase of the geometrical ratio b/h. When $b/h > 5$, the evolution of β slows down and gradually reaches a constant value whatever the material as well as the lay-up used. Thus, if $b/h > 5$, the effect of specimen thickness can be negligible;
2. For a given material and a given lay-up, the evolution of non-uniformity ratio β with the specimen width b can be described by an exponential law;
3. For a given material, specimen width and thickness, the non-uniformity value β increases linearly with the increase of material constant D_c in the range of $D_c > 0.1$;
4. For different materials, the non-uniformity ratio of unidirectional DCB specimen β_0 varies linearly with the material constant D_{c0}; however, for a multidirectional DCB specimen, the non-uniformity ratio β depends not only on its value of D_c, but also on their UD elastic constants. It is revealed that the effect of Poisson's ratio v_{12} on β can be negligible, but the non-uniformity ratio β increases as the values of E_{11} and E_{22} increase and decreases with the value of G_{13};
5. Based on the analysis of the numerical results, novel semi-empirical closed-form expressions have been proposed for rapid determination of the width-wise non-uniformity ratio β for any

uncoupled MD DCB specimen. These expressions translate the relationship between $\hat{a}$ and specimen geometrical parameters (b, h) and materials properties (E_{11}, E_{22}, G_{13}, and D_c). Good agreement between the numerical results and those from proposed formulas for different cases allows validating these propositions.

Declaration of Competing Interest

The authors declared that there is no conflict of interest.

Acknowledgement

This research work was supported by the National Natural Science Foundation of China (Grant No. 12072005, 11772028, U1864208) and the China Scholarship Council (201906020132).

Reference

[1] Karbhari, Vistasp M. "Application of composite materials to the renewal of twenty-first century infrastructure." In Proceedings of the Eleventh International Conference on Composite Materials, Gold Coast, Woodhead. 1997.

[2] Pastuszak, Przemysław D., and Aleksander Muc. "Application of composite materials in modern constructions." In Key Engineering Materials, vol. 542, pp. 119-129. Trans Tech Publications Ltd, 2013.

[3] Mangalgiri, P. D. "Composite materials for aerospace applications." Bulletin of Materials Science 22, no. 3 (1999): 657-664.

[4] Gong, Xiaojing " Rupture interlaminaire en mode mixte I+II de composites stratifiés unidirectionnels et multidirectionnels Verre/Epoxy ", Thèse de Docteur en spécialité mécanique appliquée, acoustique et matériaux, Université de Technologie de Compiègne, (1991)

[5] Gong, Xiaojing and Benzeggagh Malk, " Mixed mode interlaminar fracture toughness of unidirectional Glass/Epoxy composite ", COMPOSITE MATERIALS: Fatigue and Fracture-Fifth Volume, ASTM STP 1230, R.H. Martin, Ed., American Society for

Testing and Materials, Philadelphia, (1995), 100-123

[6] ASTM D5528-13. "Standard test method for mode I interlaminar fracture toughness of unidirectional fiber-reinforced polymer matrix composites." (2013): 1.

[7] Gong, Xiaojing, Anita Hurez, and Georges Verchery. "On the determination of delamination toughness by using multidirectional DCB specimens." Polymer testing 29, no. 6 (2010): 658-666.

[8] Shokrieh, M. M., M. Heidari-Rarani, and M. R. Ayatollahi. "Calculation of GI for a multidirectional composite double cantilever beam on two-parametric elastic foundation." Aerospace Science and Technology 15, no. 7 (2011): 534-543.

[9] Shokrieh, M. M., M. Heidari-Rarani, and S. Rahimi. "Influence of curved delamination front on toughness of multidirectional DCB specimens." Composite Structures 94, no. 4 (2012): 1359-1365.

[10] De Morais, A. B., M. F. De Moura, J. P. M. Gonçalves, and P. P. Camanho. "Analysis of crack propagation in double cantilever beam tests of multidirectional laminates." Mechanics of Materials 35, no. 7 (2003): 641-652.

[11] Davidson, B. D., and R. A. Schapery. "Effect of finite width on deflection and energy release rate of an orthotropic double cantilever specimen." Journal of Composite Materials 22, no. 7 (1988): 640-656.

[12] Davidson, Barry D. "An analytical investigation of delamination front curvature in double cantilever beam specimens." Journal of Composite Materials 24, no. 11 (1990): 1124-1137.

[13] Davidson, B. D., R. Krüger, and M. König. "Effect of stacking sequence on energy release rate distributions in multidirectional DCB and ENF specimens." Engineering Fracture Mechanics 55, no. 4 (1996): 557-569.

[14] De Morais, Alfredo Balac. "Double cantilever beam testing of multidirectional laminates." Composites Part A: Applied Science and Manufacturing 34, no. 12 (2003): 1135-1142.

[15] Samborski, Sylwester. "Numerical analysis of the DCB test configuration applicability to mechanically coupled Fiber Reinforced Laminated Composite beams." Composite

Structures 152 (2016): 477-487.

[16] Jiang, Zhengwen, Shui Wan, Zhipeng Zhong, Minghong Li, and Kongjian Shen. "Determination of mode-I fracture toughness and non-uniformity for GFRP double cantilever beam specimens with an adhesive layer." Engineering Fracture Mechanics 128 (2014): 139-156.

[17] Jiang, Zhengwen, Shui Wan, Zhipeng Zhong, Shuqin Li, and Kongjian Shen. "Effect of curved delamination front on mode-I fracture toughness of adhesively bonded joints." Engineering Fracture Mechanics 138 (2015): 73-91.

[18] Shahani, A. R., and R. Abolfathitabar. "Fracture analysis of finite length angle-ply composite double cantilever beam specimens." Proceedings of the Institution of Mechanical Engineers, Part C: Journal of Mechanical Engineering Science 233.3 (2019): 967-976.

[19] Shokrieh, M. M., and M. Heidari-Rarani. "Effect of stacking sequence on R-curve behavior of glass/epoxy DCB laminates with 0//0 crack interface." Materials Science and Engineering: A 529 (2011): 265-269.

[20] Shokrieh, M. M., M. Salamat-Talab, and M. Heidari-Rarani. "Effect of initial crack length on the measured bridging law of unidirectional E-glass/epoxy double cantilever beam specimens." Materials & Design 55 (2014): 605-611.

[21] Jumel, Julien, Michal K. Budzik, and Martin ER Shanahan. "Beam on elastic foundation with anticlastic curvature: Application to analysis of mode I fracture tests." Engineering Fracture Mechanics 78, no. 18 (2011): 3253-3269.

[22] De Gracia, J., A. Boyano, A. Arrese, and F. Mujika. "Analysis of the DCB test of angle-ply laminates including residual stresses." Theoretical and Applied Fracture Mechanics 94 (2018): 197-204.

[23] Jiang, Zhengwen, Shui Wan, Minghong Li, and Lei Ma. "Analytical solutions for non-uniformity of energy release rate of orthotropic double cantilever beam specimens with an adhesive layer." Engineering Fracture Mechanics 164 (2016): 46-59.

[24] Shokrieh, M. M, M. Heidari-Rarani, and M. R. Ayatollahi. "Interlaminar fracture toughness of unidirectional DCB specimens: A novel theoretical approach." Polymer

testing 31, no. 1 (2012): 68-75.

[25] Shokrieh, Mahmood Mehrdad, and Mohammad Heidari-Rarani. "A comparative study for beams on elastic foundation models to analysis of mode-I delamination in DCB specimens." Structural Engineering and Mechanics 37, no. 2 (2011): 149-162.

[26] Jiang, Zhengwen, Shui Wan, and Zhishen Wu. "Calculation of energy release rate for adhesive composite/metal joints under mode-I loading considering effect of the non-uniformity." Composites Part B: Engineering 95 (2016): 374-385.

[27] Zhao, Libin, Yana Wang, Jianyu Zhang, Yu Gong, Zizi Lu, Ning Hu, and Jifeng Xu. "An interface-dependent model of plateau fracture toughness in multidirectional CFRP laminates under mode I loading." Composites Part B: Engineering 131 (2017): 196-208

[28] Rybicki, Edmund F., and Melvin F. Kanninen. "A finite element calculation of stress intensity factors by a modified crack closure integral." Engineering fracture mechanics 9, no. 4 (1977): 931-938.

[29] Heidari-Rarani, Mohammad, and Mousa Sayedain. "Finite element modeling strategies for 2D and 3D delamination propagation in composite DCB specimens using VCCT, CZM and XFEM approaches." Theoretical and Applied Fracture Mechanics 103 (2019): 102246.

[30] Chou, Iton, Isao Kimpara, Kazuro Kageyama, and Isamu Ohsawa. "Mode I and mode II fracture toughness measured between differently oriented plies in graphite/epoxy composites." In Composite Materials: Fatigue and Fracture: Fifth Volume. ASTM International, 1995.